Kinetic Analysis and Ligand-Induced Conformational Changes in Dimeric and Tetrameric Forms of Human Thymidine Kinase 2[†]

João Filipe Barroso, Raquel Negrão Carvalho, and Torgeir Flatmark*

Department of Biomedicine, Section of Biochemistry and Molecular Biology, University of Bergen, Jonas Lies vei 91, N-5009 Bergen, Norway

Received October 19, 2004; Revised Manuscript Received December 23, 2004

ABSTRACT: Recombinant human thymidine kinase 2 (hTK2) expressed in *Escherichia coli* has been found to bind tightly a substoichiometric amount of deoxyribonucleoside triphosphates (dTTP > dCTP ≫ dATP), known to be strong feedback inhibitors of the enzyme. Incubation of hTK2 with the substrate dThd was able to release the dNTPs from the active site during purification from *E. coli* and thus allowed the kinetic characterization of the noninhibited enzyme, with the tetrameric hTK2 showing slightly higher activity than the most abundant dimeric form. The unliganded hTK2 revealed a lower structural stability than the inhibitor-bound enzyme forms, being more prone to aggregation, thermal denaturation, and limited proteolysis. Moreover, intrinsic tryptophan fluorescence (ITF), far-UV circular dichroism (CD), and limited proteolysis have revealed that hTK2 undergoes distinct conformational changes upon binding different substrates and inhibitors, which are known to occur in the nucleoside monophosphate kinase family. The CD-monitored thermal denaturation of hTK2 dimer/tetramer revealed an irreversible process that can be satisfactorily described by the two-state irreversible denaturation model. On the basis of this model, the parameters of the Arrhenius equation were calculated, providing evidence for a significant structural stabilization of the enzyme upon ligand binding (dCyd < MgdCTP < dThd < dCTP < dTTP < MgdTTP), whereas MgATP further destabilizes the enzyme. Finally, surface plasmon resonance (SPR) was used to study in real time the reversible binding of substrates and inhibitors to the immobilized enzyme. The binding affinities for the inhibitors were found to be 1−2 orders of magnitude higher than for the corresponding substrates, both by SPR and ITF analysis.

Thymidine kinase 2 [2′-deoxythymidine kinase (TK2, EC 2.7.1.21)][1] is a constitutively expressed enzyme that catalyzes the phosphorylation of the pyrimidines 2′-deoxythymidine (dThd), 2′-deoxycytidine (dCyd), 2′-deoxyuridine (dUrd), and their analogues to the corresponding nucleoside monophosphates, using a nucleoside triphosphate as a phosphate donor, in the presence of Mg^{2+}. Together with other deoxynucleoside kinases, TK2 is responsible for the initial and rate-limiting step of the salvage of deoxyribonucleosides in the cell, which can be further phosphorylated to triphosphates by nucleoside mono- and diphosphate kinases and eventually incorporated into DNA (reviewed in ref *1*). TK2 is predominantly a mitochondrial enzyme (*2*−*6*) but may also be present in the cytosol (*3*, *7*−*11*) and is the only dThd phosphorylating enzyme expressed in nonproliferating tissues such as liver, brain, and muscle. TK2 is thus important in providing precursors for DNA repair and/or mitochondrial DNA (mtDNA) replication in resting cells, where *de novo* synthesis is undetectable (reviewed in ref *1*). Its vital role in maintaining balanced mitochondrial deoxyribonucleoside triphosphate (dNTP) pools for mtDNA synthesis has been proven by the discovery of mutations in the *TK2* gene associated with inherited and severe mtDNA depletion syndromes (*12*−*16*). The deoxyribonucleoside kinases are preferentially feedback-regulated by the end product dNTPs of their preferred substrates, representing a fine regulatory mechanism in the maintenance of a balanced pool of dNTPs. dNTPs are considered to act as "bisubstrate analogues", with the deoxyribonucleoside moiety binding, with high specificity, to the deoxyribonucleoside-binding site of the enzyme and the triphosphate group fitting into the phosphate donor subsite (*11*, *17*−*20*).

We have previously reported the successful cloning and high-level expression of recombinant human TK2 (hTK2) in *Escherichia coli* and were able to largely improve the recovery of soluble protein by supplementation of the growth medium with ethanol and coexpression of plasmid-encoded GroEL/ES chaperonins (*11*). hTK2 was purified mainly as

[†] This work was supported by the Fundação para a Ciência e a Tecnologia (FCT), Portugal, Grants PRAXIS XXI/BD/21690/99 (to J.F.B.) and SFRH/BD/1100/2000 (to R.N.C.) and the Research Council of Norway (NFR).

* To whom correspondence should be addressed. Telephone: (+47) 55 58 64 28. Fax: (+47) 55 58 63 60. E-mail: torgeir.flatmark@biomed.uib.no.

[1] Abbreviations: TK2, thymidine kinase 2; hTK2, human TK2; hdCK, human deoxycytidine kinase; hdGK, human deoxyguanosine kinase; *Dm*-dNK, *Drosophila melanogaster* deoxynucleoside kinase; TK_{HSV1}, herpes simplex virus type-1 thymidine kinase; NMPK, nucleoside monophosphate kinase; MBP, maltose-binding protein; dThd, 2′-deoxythymidine; dCyd, 2′-deoxycytidine; dNTP, 2′-deoxyribonucleoside 5′-triphosphate; dTTP, 2′-deoxythymidine 5′-triphosphate; dCTP, 2′-deoxycytidine 5′-triphosphate; dATP, 2′-deoxyadenosine 5′-triphosphate; ATP, adenosine 5′-triphosphate; mtDNA, mitochondrial DNA; CD, circular dichroism; ITF, intrinsic tryptophan fluorescence; SPR, surface plasmon resonance; RU, resonance units; T_m, midpoint melting temperature; *h*, Hill coefficient; $[S]_{0.5}$, substrate concentration yielding half-maximum saturation.

10.1021/bi047766m CCC: $30.25
Published on Web 03/03/2005

two soluble homooligomeric forms, i.e., dimer >tetramer, containing substoichiometric amounts of dNTPs, known to be potent tight-binding feedback inhibitors of the enzyme (*11*). A detailed understanding of the catalytic and regulatory properties of hTK2 has so far been hampered by the very complex kinetics displayed with its two main substrates, dThd and dCyd, as well as the difficulties encountered in the preparation of a dNTP-free enzyme. In the present study, it is demonstrated that such an enzyme can indeed be obtained by incubation of the enzyme with high concentrations of dThd during its purification (preparative size-exclusion chromatography as a final step) from *E. coli*. The steady-state kinetics of the dNTP-free dimeric and tetrameric forms revealed interesting new kinetic parameters and regulatory properties as well as some differences between the two oligomeric forms. Moreover, affinities and conformational changes associated with the binding of substrates and inhibitors have been studied by intrinsic tryptophan fluorescence (ITF), far-UV circular dichroism (CD), surface plasmon resonance (SPR), and limited tryptic proteolysis.

EXPERIMENTAL PROCEDURES

Expression and Purification of Recombinant hTK2. hTK2 was expressed as a fusion protein in *E. coli* [BL21*trxB*(DE3) cells], with maltose-binding protein (MBP) as the stabilizing fusion partner (MBP-(pepIEGR)$_{Xa}$-hTK2), together with the molecular chaperones GroEL/ES (*11*). Cells were grown at 37 °C, and expression was induced at 28 °C by the addition of 1 mM isopropyl thio-β-D-galactoside (IPTG). Ethanol was added to the medium prior to inoculation at a 3% (v/v) final concentration. The cells were harvested after 24 h of induction. After protein purification by affinity chromatography (amylose resin, 4 °C), the fusion protein was cleaved overnight (approximately 16 h) at 4 °C either in the presence or absence of 1 mM dThd by the restriction protease factor Xa (Protein Engineering Technology ApS) using a protease/hTK2 ratio of 1:150 (w/w). Tetrameric hTK2 was directly isolated by size-exclusion chromatography at 4 °C using a HiLoad Superdex 200 HR column (1.6 × 60 cm) prepacked from Amersham Biosciences, and the peak fraction containing both dimeric hTK2 and MBP was sequentially applied to a second column of amylose resin, to remove MBP (*11*). Dimeric hTK2 was further isolated by a second size-exclusion chromatography step. Aliquots of purified tetrameric/dimeric hTK2 were stored in liquid nitrogen until used. The protein concentration was determined by the Bradford protein assay (Bio-Rad), using bovine serum albumin (BSA) as the standard, and sample purity was checked by 15% SDS−PAGE.

Chromatographic Analysis of Bound Deoxyribonucleotides. The dNTPs bound to hTK2 were released from the protein by 4% (w/v) perchloric acid precipitation and identified/quantified by anion-exchange HPLC analysis as previously described (*11*).

Assay of hTK2 Activity. The hTK2 activity was assayed as described previously (*11*) except that the concentration of enzyme was reduced to 0.2 or 0.5 μg/mL (because of the higher specific activities than those for the dNTP-inhibited enzyme), for the dThd and dCyd titrations, respectively. The steady-state enzyme kinetic parameters were calculated by nonlinear regression analysis using the SigmaPlot Technical Graphing Software (SPSS Inc.) and the Hill equation. In some experiments, the time course of the reaction was followed to study the effect of substrate preincubation on the specific activity of the enzyme as previously described (*11*).

Limited Proteolysis by Trypsin. Limited proteolysis of the dimeric hTK2 (0.66 mg/mL) by trypsin was performed at 25 °C and a protease/hTK2 ratio (by mass) of 1:50 for the inhibited enzyme. Under the same experimental conditions, the rate of proteolysis of the noninhibited enzyme was too high to be followed in the same time scale and therefore a protease/hTK2 ratio (by mass) of 1:100 was used instead for this enzyme preparation. At timed intervals (0−120 min), aliquots were taken from the proteolytic reaction, quenched with SDS denaturation buffer by heating for 5 min at 95 °C, and subjected to SDS−PAGE analysis and the band corresponding to the full-length subunit was quantified. The effect of the substrate dThd (300 μM) on the extent of proteolysis of the enzyme was also studied.

Far-UV CD. Dimeric and tetrameric dNTP-free hTK2 samples (8−10 μM subunit) were prepared in 20 mM Hepes and 200 mM NaCl (pH 7.0), unless otherwise stated, and placed in quartz cells with a 0.1 cm path length. For comparison, "endogenously inhibited" dimeric and tetrameric hTK2 samples were also studied. When indicated, ligands were added to the protein solution to study the effect of substrates (dThd and dCyd), cosubstrate (MgATP), and inhibitors (MgdCTP/dCTP and MgdTTP/dTTP) on the secondary structure and conformational stability of the enzymes. In some experiments where Mg^{2+} was to be excluded, measurements were made in the presence of 1 mM EDTA. CD spectra in the far-UV range were recorded at 25 °C on a computer-controlled Jasco J-810 spectropolarimeter equipped with a Jasco PTC-423S Peltier element for temperature control. Wavelength scans were taken between 185/200 and 260 nm, and buffer/ligand scans were routinely recorded and subtracted from the protein spectra. The spectra reported are averages of four scans taken at a scan rate of 20 nm/min and were all smoothed using the J-810 noise reduction software. Estimation of secondary structure elements was performed using the neural net algorithm (CDNN) of Andrade et al. (*21*). The global conformational stability, as measured by thermal denaturation (range 20−90 °C), was monitored by following the changes in ellipticity at 222 nm at a constant heating rate of 40 °C/h. Reversibility of the thermal transition was checked by recording the CD signal while cooling a hTK2 sample from 90 °C to 20 °C. Individual hTK2 melting curves were fitted to the two-state irreversible model (*22*) using a nonlinear least-squares fit routine with the SigmaPlot Technical Graphing Software (SPSS Inc.). The equation describing any general spectroscopic signal Y observable at a particular temperature under a given set of conditions for a transition between two physical states can be expressed as

$$Y = Y_U - f_N(Y_U - Y_N) \quad (1)$$

where f_N is the fraction of molecules remaining in the native state as a function of the temperature and Y_N and Y_U are the signals contributed by the native and unfolded states, respectively. The signal for a given state will usually change with a change in temperature. Thus, in the analysis of a

thermal unfolding profile, the baseline of the observable signal is frequently observed to have a slope m_N for the native state and m_U for the unfolded state, which must be included in the fitting process

$$Y = m_U T + Y_U - f_N[(m_U T + Y_U) - (m_N T + Y_N)] \quad (2)$$

In the case of the two-state irreversible model, in which only the native (N) and final (irreversibly denatured) (D) states are significantly populated and the conversion from N to D is determined by a strongly temperature-dependent, first-order rate constant (k) that changes with temperature, as given by the Arrhenius equation ($k = \exp\{(E_A/R)(1/T_m - 1/T)\}$), the value of f_N is given by (*22*)

$$f_N = \exp\left\{-\frac{1}{\upsilon}\int_{T_0}^{T} \exp\left[\frac{E_A}{R}\left(\frac{1}{T_m} - \frac{1}{T}\right)\right] dT\right\} \quad (3)$$

where $\upsilon = dT/dt$ (K min^{-1}) is a scan rate value, E_A is the Arrhenius activation energy of the denaturation process, R is a gas constant, T is the absolute temperature, and T_m is the midpoint melting temperature (in kelvin), where k is equal to 1 min^{-1}.

The apparent midpoint melting temperature (T_m) values of endogenously inhibited hTK2 were determined from the first/second derivatives of the denaturation curves after noise reduction by using the standard analysis program provided with the instrument. The first derivative profiles were further resolved (deconvoluted) into individual T_m transitions, using a Gaussian distribution function in the PeakFit software program (SPSS Inc.).

Intrinsic Tryptophan Fluorescence (ITF) Measurements. The ITF of hTK2 was measured on a Perkin−Elmer LS-50B instrument at 25 °C in a buffer containing 20 mM Hepes and 200 mM NaCl (pH 7.0) and a protein concentration of 0.03 mg/mL. The excitation and emission wavelengths used were 295 and 338 nm, respectively. hTK2 was excited at 295 nm because the presence of eight tyrosines in this enzyme makes a significant contribution to the observed fluorescence when excited at wavelengths less than 290 nm. To study the effect of the substrates or inhibitors, increasing concentrations (0.05−2000 μM) of dThd, dCyd, MgATP, MgdTTP, MgdCTP (2:1 $MgCl_2$/(d)NTP ratio), dTTP, or dCTP were added to the incubation mixture every time equilibrium was achieved after the previous addition and the change in fluorescence intensity (ΔF_{338}) was measured as a function of the concentration of added ligand. In each experiment the fluorescence intensity was corrected for dilutions because of ligand addition, which did not exceed 10% in any case. Background emission (<5%) was eliminated by subtracting the signal from buffer containing the appropriate quantity of ligand. Nonlinear regression analysis of the data (the binding isotherm) was performed using the SigmaPlot Technical Graphing Software (SPSS Inc.) and the Hill equation.

SPR Analysis. Real-time interaction analyses between immobilized enzyme and its different substrates and inhibitors (analytes) were performed by SPR analysis using the Biacore 3000 biosensor instrument (Biacore AB, Uppsala, Sweden). Dimeric hTK2, with bound dNTP inhibitors (*11*), was diluted ~30 times in 10 mM sodium acetate buffer (pH 5.5) to a final concentration of 0.21 mg/mL and immobilized covalently to the hydrophilic carboxymethylated dextran matrix of a CM5 sensor chip by the standard primary amine coupling reaction, as described by the manufacturer. The amount of immobilized protein was estimated from the increase in ΔRU (change in resonance units) by assuming that 1000 RU correspond to ~1 ng of immobilized protein/mm^2 (*23*), and an average surface concentration of 17.64 ± 0.76 ng/mm^2 (ΔRU of 17 640 ± 760 RU) was obtained. A reference surface was subjected to the same procedure but with no protein to correct for any unspecific binding of the analytes together with changes in the bulk refractive index. Equilibration of the baseline (drift < −0.05 RU/s) was obtained by a continuous flow (30 μL/min) of HBS-N buffer (10 mM Hepes and 150 mM NaCl at pH 7.4) for ~2 h together with several injections of dThd followed by MgATP over the immobilized hTK2 to release any bound dNTP inhibitors. All biosensor analyses were performed at 25 °C with HBS-N running buffer at a constant flow of 30 μL/min. Each analyte was dissolved in running buffer and analyzed using a ~10^6 dilution series, i.e., dThd (0.001−2000 μM), dCyd (0.005−2000 μM), MgATP (0.005−2000 μM), MgdTTP/dTTP, and MgdCTP/dCTP (0.001−1000 μM). Unless otherwise stated, the cosubstrate ATP and the inhibitors were used in the presence of Mg^{2+}, in a 2:1 $MgCl_2$/(d)NTP ratio. A new sensor chip was used for each titration experiment. Although the immobilized enzyme was very stable, a standard concentration of each analyte was injected at different time points of the experimental period and the low rate of decay of that signal was used to correct the measured SPR responses for each analyte concentration. All of the compounds dissociated back to the baseline within a relatively short time frame, but a regeneration step with a 3 min injection of 100 μM dCyd was performed after each dNTP injection. All sensorgrams were processed by first subtracting the binding response recorded from the control surface. The equilibrium SPR response at $t = 3$ min and the apparent half-time for the off rates were measured directly from the sensorgrams. To account for different immobilization levels of enzyme, the SPR response to analyte binding in each sensorgram was expressed as ΔRU/(ng of hTK2/mm^2). The concentration of analyte at half-maximum response ($[S]_{0.5}$) was calculated from the derived equilibrium binding isotherms by nonlinear regression analysis using the SigmaPlot Technical Graphing Software (SPSS Inc.) and the Hill equation.

RESULTS

Preparation of dNTP-free Enzyme. Given the previously reported preparation of recombinant hTK2, purified with bound endogenous inhibitors (dTTP, dCTP, and a minor amount of dATP), it was important to develop a method for the efficient removal of these compounds, to obtain the kinetic properties of the noninhibited enzyme and to determine the affinities for the substrates and inhibitors. In this study, we were able to remove all of the bound dNTPs from the purified recombinant hTK2 by incubation of the enzyme with a high concentration of the substrate dThd, followed by a single step of preparative size-exclusion chromatography, as determined by anion-exchange HPLC of the perchloric acid precipitated isolated dimer and tetramer (data not shown). The oligomeric state of the enzyme reported in our previous work (*11*), i.e., dimers, tetramers, hexamers,

Table 1: Steady-State Kinetic Constants of dNTP-free Recombinant Human TK2[a]

	dThd			dCyd			MgATP		
enzyme	$[S]_{0.5}$ (μM)	V_{max} (nmol min^{-1} mg^{-1})	h	K_m (μM)	V_{max} (nmol min^{-1} mg^{-1})	h	K_m (μM)	V_{max} (nmol min^{-1} mg^{-1})	h
dimer	5.8 ± 2.0	998 ± 57	0.37 ± 0.03	4.0 ± 0.1	463 ± 3	0.95 ± 0.02	2.8 ± 0.1	785 ± 6	0.87 ± 0.03
tetramer	6.5 ± 0.8	1261 ± 32	0.54 ± 0.02	4.9 ± 0.2	732 ± 7	0.83 ± 0.02	5.9 ± 0.4	1081 ± 14	0.78 ± 0.03

[a] The values were from four independent assays. The kinetic parameters were calculated by nonlinear regression analysis of the experimental data using the Hill equation. The concentrations of dThd and dCyd were varied from 0.05 to 300 μM, with the ATP concentration kept constant at 300 μM (600 μM $MgCl_2$), and the ATP concentration was varied from 0.1 to 2000 μM (2:1 $MgCl_2$/ATP ratio), with the dThd concentration kept constant at 200 μM. The $[S]_{0.5}$ values represent the dThd concentration at half-maximal activity. The Hill coefficients (h) calculated from Hill plots using the V_{max} values given from curve fitting matched the ones obtained by nonlinear regression analysis, in all of the substrate concentration range.

and some higher molecular mass forms (aggregates), was observed also after the removal of the dNTP inhibitors, as determined by preparative and analytical size-exclusion chromatography. The recovery of soluble tetrameric and dimeric forms, i.e., 3−4 mg/L of bacterial culture, represented about one-third of the total amount of endogenously inhibited enzyme obtained when no preincubation with dThd was performed (*11*). On analytical (HPLC) size-exclusion chromatography of the liquid N_2 stored isolated enzyme preparations, the dimer revealed ~18% cross-contamination with the tetramer and the tetramer revealed ~26% cross-contamination with dimer at the time of analysis, but higher molecular mass forms (aggregates) were absent from both preparations.

Steady-State Kinetic Analysis. The dNTP-free dimeric and tetrameric hTK2 revealed linear time courses for both the substrates dThd and dCyd when measured up to 15 min at 25 °C, and no differences were observed whether no preincubation or 5 min of preincubation with the substrate or cosubstrate (MgATP) were performed prior to initiation of the reaction (data not shown). As seen from Table 1 and Figure 1, our dNTP-free dimeric and tetrameric enzyme preparations followed near Michaelis−Menten kinetics for MgATP ($h = 0.87$ and 0.78, respectively) and dCyd ($h = 0.95$ and 0.83, respectively), while for dThd, a strong negative cooperativity was observed, with Hill coefficients of $h = 0.37$ and 0.54 for the dimeric and tetrameric hTK2, respectively. Hill plots of the kinetic data, using the calculated V_{max} values, were linear and gave similar values as the ones obtained by nonlinear regression analysis (Figure 1). Overall, the dimeric enzyme is less active than the tetramer (~1.4 times lower V_{max} values) and shows a stronger negative cooperativity with dThd as the variable substrate (Table 1). hTK2 has similar apparent affinities for the substrates dThd and dCyd and the cosubstrate MgATP, although the dimeric form shows slightly higher affinities for the three ligands than the tetrameric enzyme. Thus, the catalytic efficiency ($k_{cat}/[S]_{0.5}$) of the tetramer is ~1.2-fold higher than for the dimer. Moreover, the catalytic efficiency of the dNTP-free dimeric and tetrameric hTK2 increased 16−18-fold with dThd and 10−11-fold with dCyd as the variable substrate when compared to the previously characterized dNTP-inhibited enzymes (*11*). Finally, as previously observed for the endogenously inhibited enzyme (*11*), the specific activity of both dNTP-free dimer and tetramer showed a ~3-fold increase when measured at 37 °C as compared to 25 °C (data not shown).

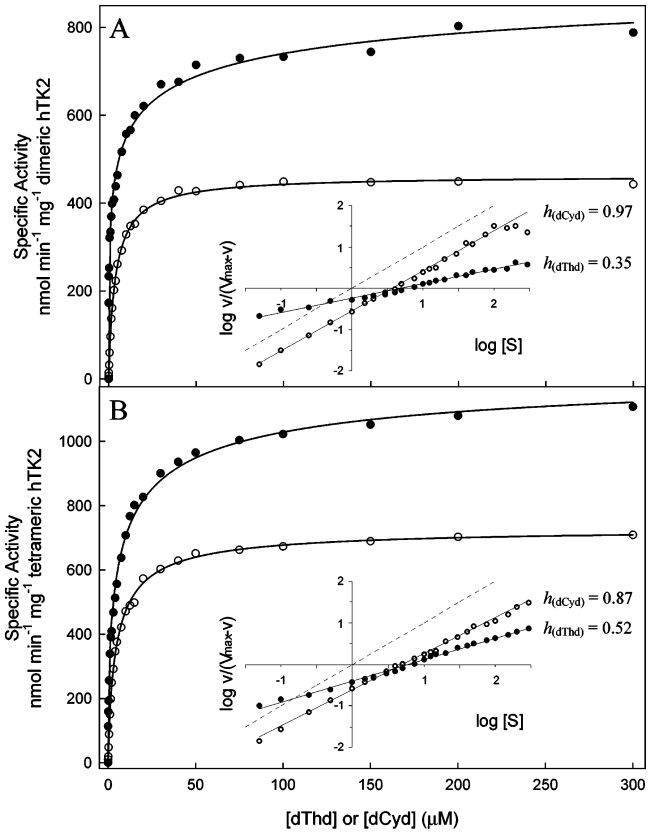

FIGURE 1: Catalytic activity of recombinant hTK2 at varied concentrations of dThd and dCyd. For assay conditions and nonlinear regression analysis, see the Experimental Procedures. (A) hTK2 dimer with dThd (●) or dCyd (○) as the variable substrate. (B) hTK2 tetramer with dThd (●) or dCyd (○) as the variable substrate. The fitted curves were obtained using the Hill equation and nonlinear regression analysis. The insets show Hill plots of the same data, with the dashed line indicating a Hill coefficient of 1.0. For all linear regressions, the correlation coefficient (r^2) was equal to or greater than 0.99. The steady-state kinetic constants are summarized in Table 1.

Limited Proteolysis by Trypsin. Limited proteolysis of proteins in a close-to-native state is a powerful tool to probe changes in the higher-order structure in response, for example, to ligand binding (*24*). In this study, we have probed substrate-induced conformational changes both on the dNTP-free and the endogenously inhibited enzymes. Time-course studies revealed that the dimeric dNTP-free hTK2 was more susceptible to limited proteolysis by trypsin than the dimeric enzyme copurified with the endogenous inhibitors dTTP and dCTP (*11*), even when proteolyzed at a lower trypsin/enzyme ratio (1:100 and 1:50, by mass,

respectively), with about 32.4 ± 2.8 and 58.4 ± 1.6% of the full-length protomer recovered after incubation for 2 h for the dNTP-free and dNTP-inhibited forms, respectively (data not shown). Moreover, while incubation of the non-inhibited enzyme with dThd decreased the rate of proteolysis, with 42.4 ± 2.1% of the full-length protomer recovered after incubation for 2 h, the tryptic cleavage of the dNTP-inhibited hTK2 was enhanced on incubation with dThd, with only 37.6 ± 1.8% of the full-length recovered.

Far-UV CD. The far-UV CD spectra observed for dimeric and tetrameric hTK2 were similar and contain two minima at 210 and 221 nm and a maximum at 194 nm (when measured in phosphate buffer) (data not shown), as previously reported for the related enzyme TK_{HSV1} (*25*), which is characteristic of proteins with a high α-helical content. The secondary structure content of the ligand-free hTK2 estimated from the CD spectra obtained in phosphate buffer (185−260 nm) was 40.0 ± 1.6% α helix, 12.8 ± 1.3% β sheet, 15.5 ± 0.3% β turn, and 30.7 ± 1.2% random coil. Unfortunately, the high absorbance of the nucleosides and nucleotides in the far-UV region resulted in high noise levels, which hampered satisfactory data collection at $\lambda < 205$ nm and proper deconvolution of the CD spectra by CDNN. Nevertheless, no significant changes in the spectra seem to take place upon binding of any ligand to dimeric or tetrameric hTK2 (data not shown). The thermal denaturation profile followed at $\lambda = 222$ nm could, however, be used to assess the conformational state of the enzyme in its ligand-free and ligand-bound forms. hTK2 undergoes an irreversible thermal denaturation with a single transition as seen from the sigmoidal decrease in the negative ellipticity at 222 nm and the shape of the denaturation curve, which was essentially symmetric (Figure 2). In all cases (absence or presence of ligands), the thermal denaturation of hTK2 was accompanied by an aggregation. To check the irreversibility, a heating scan was stopped at 59 °C, when unfolding of the ligand-free enzyme is completed, and cooled back to 20 °C, but no signal was recovered (data not shown). Because of the irreversible character of hTK2 denaturation, we analyzed the transition curves in terms of a simple two-state irreversible model (Figures 2 and 3) (see the Experimental Procedures). Dimeric and tetrameric hTK2 showed approximately the same transition temperature (T_m) values (with a maximal variation of ±2 °C) for all of the ligands tested, but the apparent Arrhenius activation energies (E_A) for the process were always higher for the tetrameric enzyme (Table 2). The ligand-free dimeric hTK2 in Hepes buffer denatured with a T_m value of 54.2 ± 0.1 °C, whereas in KH_2PO_4 buffer, the enzyme was stabilized by a ΔT_m of +3.4 °C. The addition of the cosubstrate ATP also demonstrated a certain stabilizing effect ($\Delta T_m \approx +2$ °C), whereas in the presence of magnesium (MgATP) a ~5 °C decrease in the T_m value was observed. Both substrates, dThd and dCyd, had a stabilizing effect, shifting the T_m value of dimeric hTK2 to 66.3 ± 0.1 and 60.0 ± 0.1 °C, respectively. The simultaneous addition of substrate (dThd or dCyd) and cosubstrate ATP (in the presence of EDTA to suppress any enzymatic activity) resulted in only a slight stabilization ($\Delta T_m \approx +1$ °C) when compared to the substrate-bound enzyme. The feedback inhibitors dTTP and dCTP showed an even more pronounced thermal stabilization of the enzyme, and inclusion of magnesium changed the denaturation profile differently for the two dNTP-bound hTK2 forms; i.e., it was stabilized by a ΔT_m of ~ +3 °C further from the 76.8 ± 0.2 °C found for the hTK2·dTTP complex and destabilized by a ΔT_m of ~ −8 °C from the 71.8 ± 0.2 °C found for the hTK2·dCTP complex (Table 2). These results fit in well with the biphasic thermal denaturation profile obtained for the endogenously inhibited dimeric hTK2 containing substoichiometric amounts of dNTPs (mainly dTTP and dCTP), with apparent T_m values of 56.0 ± 1.1 and 68.0 ± 1.0 °C (Figure 3). Incubation of the endogenously inhibited dimeric enzyme with the substrates or cosubstrate induced apparent single transitions, with T_m values of 62.9 ± 1.0 °C for dThd, 59.7 ± 1.3 °C for dCyd, and 55.3 ± 1.1 °C for MgATP (Table 2). The endogenously inhibited hTK2 tetramer revealed an apparent single transition temperature at 61.9 ± 1.1 °C (Figure 3B) but similar transitions as the dimeric enzyme upon incubation with substrates or cosubstrate (Table 2).

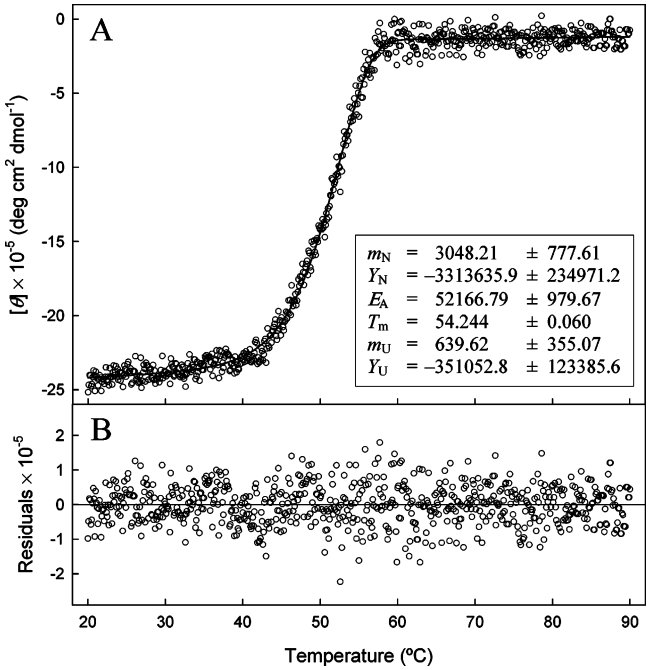

FIGURE 2: Fit of the CD-monitored thermal denaturation profile of ligand-free dimeric hTK2 (0.23 mg/mL) in 20 mM Hepes and 200 mM NaCl (pH 7.0) to the two-state irreversible model described by eqs 2 and 3. For assay conditions and nonlinear regression analysis, see the Experimental Procedures. (A) (○) represents the CD signal of hTK2 at 222 nm as a function of the temperature, and (—) represents the fitted curve to the experimental data. The fitted parameters describing the data set are shown in the inset and represent the slope m_N and intercept Y_N of the native-state baseline, the midpoint melting temperature T_m (°C), the Arrhenius activation energy of the denaturation process E_A (cal mol^{-1}), and the slope m_U and intercept Y_U of the unfolded state baseline. (B) Residuals for the irreversible two-state fit shown in A, representing the differences between the predicted and measured values. [θ], molar ellipticity.

ITF Measurements. hTK2 has five tryptophan residues, at positions 55, 74, 133, 136, and 189. Four of these residues are absolutely conserved in the deoxynucleoside kinases *Dm*-dNK, hdCK, and hdGK, and Trp136 is a phenylalanine in the *Dm*-dNK and hdGK enzymes. On the basis of the structure of hdCK (*26*), three of these residues are located at the dimer interface (Trp74, Trp133, and Trp136), one at the active site (Trp55) establishing a $\pi-\pi$ stacking interaction with the substrate/inhibitor base, and the last (Trp188) is localized at the end of α-helix 9 following the LID region.

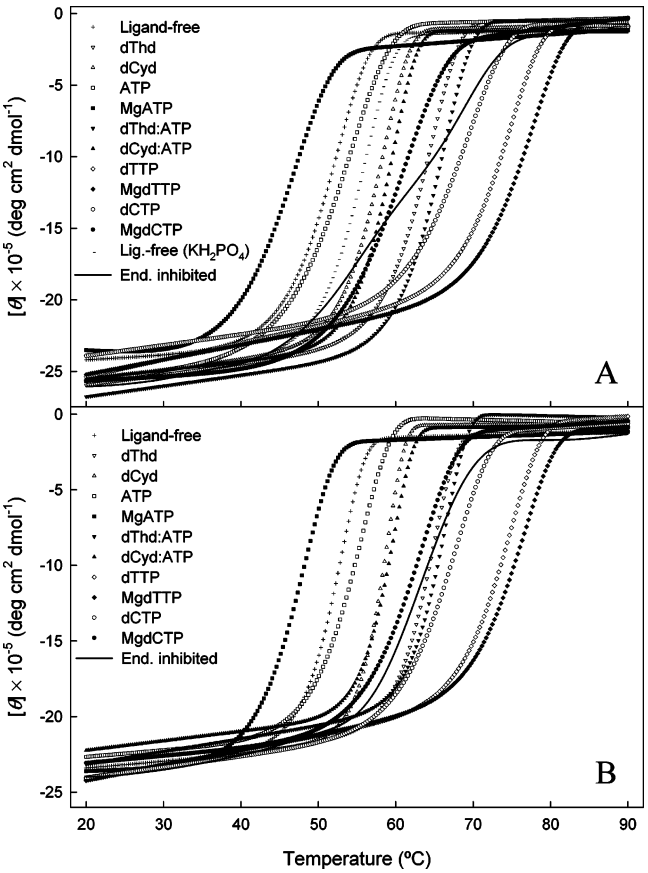

FIGURE 3: CD-monitored thermal denaturation profiles of ligand-free and ligand-bound hTK2 (0.23 mg/mL) obtained by a nonlinear fit routine of the experimental data to the two-state irreversible model described by eqs 2 and 3. The CD signal was recorded at 222 nm as a function of temperature for dimeric (A) and tetrameric (B) hTK2. The melting curves for noninhibited hTK2 were obtained in 20 mM Hepes and 200 mM NaCl (pH 7.0) in the absence of ligand (+), with 300 μM dThd (▽), 300 μM dCyd (△), 300 μM ATP (□), 300 μM MgATP (■), 300 μM dThd and 300 μM ATP (▼), 300 μM dCyd and 300 μM ATP (▲), 300 μM dTTP (◇), 300 μM MgdTTP (◆), 300 μM dCTP (○), 300 μM MgdCTP (●), and 20 mM KH_2PO_4 and 50 mM KF (pH 7.0) in the absence of ligand (−). The fitted parameters are summarized in Table 2. For comparison, the melting curves for the endogenously inhibited dimeric (A) and tetrameric (B) hTK2 (—) after noise reduction are also shown. In this case, the transition temperatures (Table 2) were determined from the first derivative of the denaturation profile. [θ], molar ellipticity.

In hTK2, one or several of these tryptophans may be involved in the conformational changes associated with the binding of different ligands to the enzyme, as followed by ITF. dThd and dCyd induced a quenching of the fluorescence emission at a λ_{max} of 338 nm (no shift in emission maximum), and their binding isotherms displayed a near hyperbolic concentration dependence ($h = \sim 0.8$) (Table 3), with the $[S]_{0.5}$ value for dCyd (1.4−1.5 μM) being ~3-fold lower than for dThd (4.1−4.5 μM), for both oligomeric forms (data for tetrameric hTK2 not shown). The dimeric form seems to adopt different conformational states at different concentration ranges of the cosubstrate MgATP. Thus, in the range of 0.05−4 μM, a decrease in the fluorescence quantum yield was observed with $[S]_{0.5}$ of 0.5 ± 0.1 μM ($h = 1.3 \pm 0.2$); at concentrations up to 100 μM, dimeric hTK2 revealed an increase in the ITF with $[S]_{0.5}$ of 14.5 ± 0.3 μM ($h = 1.4 \pm 0.05$) (Table 3), and at even higher concentrations, a new quenching phase of the ITF was observed (data not shown). The addition of MgATP to the tetrameric enzyme resulted in similar ITF responses as for the dimeric enzyme but with significantly lower ΔF signals. A slight positive cooperativity was observed for the quenching by both MgdTTP and MgdCTP, with lower $[S]_{0.5}$ values (0.4 ± 0.01 and 0.2 ± 0.01 μM, respectively) than those for the substrates dThd or dCyd. For both inhibitors, exclusion of magnesium did not significantly change the equilibrium binding isotherms for either the dimeric or tetrameric form (data not shown).

SPR Analysis. The endogenously (dNTP) inhibited enzyme was selected for immobilization because of its higher stability on short-term exposure to pH 5.5 compared to the isolated dNTP-free recombinant enzyme. The dimeric form was immobilized to an average ΔRU value of 17 640 ± 760 RU, which corresponds to 17.6 ± 0.8 ng of immobilized enzyme/mm^2. After immobilization, a ligand-free enzyme was obtained by repeated injections of 300 μM dThd. A final injection of 5 μM MgATP further improved the stability of the baseline. This resulted in satisfactory binding responses [0.9−5.0 ΔRU_{max}/(ng of immobilized enzyme/mm^2)] for all of the analytes (Table 4). An influence of mass transport was excluded for the low-molecular-mass analytes (227−507 Da) at the selected high flow rate (30 μL/min).

The sensorgrams for all of the analytes were analyzed using the BIAevaluation software supplied with the instrument, but systematic deviations from the available binding models were observed. Therefore, the sensorgrams were all analyzed by a simple Langmuir binding isotherm, and the association equilibrium signal (ΔRU at $t = 3$ min) (Figure 4) as a function of the free analyte concentration was used to determine the apparent affinities and the maximum SPR signals [ΔRU_{max}/(ng/mm^2)] by nonlinear regression analysis (Table 4). dTTP and dCTP revealed the highest apparent affinities, with half-maximum saturation ($[S]_{0.5}$) at 88 ± 15 and 38 ± 3 nM, respectively (Table 4). Interestingly, the presence of Mg^{2+} markedly reduced their apparent affinity, with $[S]_{0.5}$ values of 14.6 ± 2.6 and 5.7 ± 4.1 μM found for MgdTTP and MgdCTP, respectively. In comparison, the substrates dThd, dCyd, and cosubstrate MgATP gave the $[S]_{0.5}$ values of 0.5 ± 0.2, 9.8 ± 1.2, and 2.5 ± 0.4 μM, respectively (Table 4). Moreover, the strong negative kinetic cooperativity with dThd ($h = 0.37$) was confirmed by the SPR analysis ($h = 0.31$).

Further comparative analyses of the sensorgrams (Figure 4) were most easily interpreted in the dissociation phase, which is essentially a function of the dissociation rate. The time course for the dCyd response revealed a "square-wave" pattern; i.e., the full SPR response was reached within seconds, and it returned rapidly (<1 s) to the baseline level at the end of the injection cycle (Figure 4B), as expected from simple binding of a low-molecular-mass analyte with relatively low affinity (*27*). In contrast, all of the other compounds revealed a time-dependent SPR response for both the association and dissociation phases, notably in the lower concentration range (parts A and C−F of Figure 4). Whereas the rapid dissociation rate for dCyd was too fast to measure the half-time, the dissociation rate for dThd was relatively slow, with a half-time of 12.0 ± 1.8 s at a high concentration of the analyte. The cosubstrate MgATP gave a half-time of 3.4 ± 0.4 s, i.e., similar to the inhibitors MgdTTP ($t_{1/2,obs}$ off = 4.2 ± 0.8 s) and MgdCTP ($t_{1/2,obs}$ off = 5.6 ± 1.5 s).

Table 2: Arrhenius Equation Parameter Estimates for the Two-State Irreversible Model of the Thermal Denaturation of hTK2

	hTK2 dimer		hTK2 tetramer	
hTK2 ligand	T_m (°C)	E_A (kcal mol^{-1})	T_m (°C)	E_A (kcal mol^{-1})
ligand-free	54.24 ± 0.06	52.17 ± 0.98	54.29 ± 0.05	71.43 ± 1.33
ligand-free (KH_2PO_4)	57.57 ± 0.05	61.28 ± 0.92		
dThd	66.26 ± 0.08	63.11 ± 1.27	66.19 ± 0.07	79.23 ± 1.75
dCyd	59.95 ± 0.07	67.75 ± 1.63	59.89 ± 0.05	98.80 ± 2.22
ATP[a]	56.52 ± 0.10	43.24 ± 1.09	57.25 ± 0.08	57.91 ± 1.41
MgATP[b]	48.99 ± 0.10	41.93 ± 1.27	49.88 ± 0.07	54.84 ± 1.45
dThd/ATP[a]	67.87 ± 0.11	65.41 ± 1.82	67.72 ± 0.09	82.63 ± 2.45
dCyd/ATP[a]	61.03 ± 0.07	73.56 ± 1.79	60.87 ± 0.09	87.29 ± 3.21
dTTP[a]	76.82 ± 0.21	61.60 ± 1.91	76.61 ± 0.16	62.97 ± 1.62
MgdTTP[b]	79.93 ± 0.27	58.31 ± 1.49	78.47 ± 0.19	60.86 ± 1.47
dCTP[a]	71.83 ± 0.18	48.81 ± 1.38	69.83 ± 0.14	53.31 ± 1.38
MgdCTP[b]	63.48 ± 0.13	41.51 ± 1.05	65.41 ± 0.11	49.75 ± 1.21
endogenous inhibited[c]	56.0 ± 1.1, 68.0 ± 1.0	nd	61.9 ± 1.1	nd
dThd[c]	62.9 ± 1.0	nd	63.4 ± 0.9	nd
dCyd[c]	59.7 ± 1.3	nd	60.3 ± 1.3	nd
MgATP[b,c]	55.3 ± 1.1	nd	56.1 ± 1.3	nd

[a] Measurements done in the presence of 1 mM EDTA. [b] 2:1 $MgCl_2$/(d)NTP ratio. [c] For the endogenous inhibited enzyme in the presence or absence of extra ligands (dThd, dCyd, or MgATP), the T_m values were obtained by deconvolution of the first derivative of the melting curves. In the absence of extra ligands, the endogenous inhibited dimeric enzyme showed a biphasic thermal transition (Figure 3).

Table 3: Kinetic Parameters for the Equilibrium Binding of Substrates and Inhibitors to Dimeric hTK2 as Determined by Changes in ITF[a]

ligand	ΔF_{max}	$[S]_{0.5}$ (μM)	h
dThd	(−) 134.4 ± 4.4	4.1 ± 0.4	0.80 ± 0.04
dCyd	(−) 132.0 ± 2.1	1.4 ± 0.1	0.76 ± 0.03
MgATP[b,c]	(−) 33.2 ± 1.6	0.5 ± 0.1	1.3 ± 0.2
	(+) 68.6 ± 0.9	14.5 ± 0.3	1.4 ± 0.05
MgdTTP[c]	(−) 112.3 ± 1.0	0.42 ± 0.01	1.57 ± 0.05
MgdCTP[c]	(−) 120.5 ± 1.2	0.21 ± 0.01	1.63 ± 0.07

[a] The values were from two independent assays. The parameters were calculated by nonlinear regression analysis of the experimental data using the Hill equation. The concentration ranges of ligand used in the fit were 0.05−50 μM for dThd and dCyd, 0.05−100 μM for MgATP, and 0.05−10 μM for MgdTTP and MgdCTP. The $[S]_{0.5}$ values represent the concentration of ligand that gave a half-maximum steady-state equilibrium ITF response. For maximum steady-state equilibrium ITF response (ΔF_{max}), (−) indicates quenching and (+) indicates an increase in the quantum yield of fluorescence intensity upon ligand addition. [b] MgATP induced a quenching of the ITF of hTK2 in the concentration range 0.05−4 μM, but an increase in the quantum yield in the concentration range 5−100 μM and, thus, the upper and lower parameters presented correspond to independent fits of the experimental data obtained in each of the concentration series, respectively. [c] 2:1 $MgCl_2$/(d)NTP ratio.

Table 4: Kinetic Parameters for the Substrate- and Inhibitor-Induced Changes in the Refractive Index (ΔRU) of Immobilized Dimeric hTK2 as Measured by SPR[a]

analyte	ΔRU_{max}/ (ng/mm^2)	$[S]_{0.5}$ (μM)	h	$t_{1/2,obs}$ off (s)
dThd	3.3 ± 0.1	0.5 ± 0.2	0.31 ± 0.03	12.0 ± 1.8
dCyd	4.2 ± 0.2	9.8 ± 1.2	0.74 ± 0.03	nd
MgATP[b]	4.3 ± 0.2	2.5 ± 0.4	0.67 ± 0.04	3.4 ± 0.4
MgdTTP[b]	5.0 ± 0.2	14.6 ± 2.6	0.47 ± 0.01	4.2 ± 0.8
dTTP	1.35 ± 0.04	0.088 ± 0.015	0.35 ± 0.02	7.5 ± 0.9
MgdCTP[b]	3.9 ± 0.5	5.7 ± 4.1	0.35 ± 0.03	5.6 ± 1.5
dCTP	0.93 ± 0.01	0.038 ± 0.003	1.2 ± 0.1	24.8 ± 1.3

[a] The values were from two independent assays. The parameters were calculated by nonlinear regression analysis of the experimental data (binding isotherms) using the Hill equation. The concentration ranges of analyte used in the fit were 0.001−50 μM for dThd, MgdTTP, dTTP, MgdCTP, and dCTP and 0.05−50 μM for dCyd and MgATP. The $[S]_{0.5}$ values represent the concentration of analyte that gave a half-maximum steady-state equilibrium SPR response. The apparent $t_{1/2,obs}$ off values represent the half-time for the overall ΔRU off-response as measured directly from the sensorgrams. [b] 2:1 $MgCl_2$/(d)NTP ratio.

The experimental error for the SPR response in replicate injections of the analyte was found to be <4% in two independent titration experiments. Finally, the specificity of the SPR signal responses shown in Figure 4 was verified by injecting the nonsubstrate nucleoside deoxyguanosine (dGuo), with no observable signal being obtained at concentrations up to 20 μM (data not shown).

DISCUSSION

dNTP-free hTK2 and Its Oligomeric Forms. Previous biochemical characterization of recombinant hTK2 in this laboratory was performed with an enzyme isolated from *E. coli* with a substoichiometric amount of inhibitory endogenous dNTPs (∼0.8 mol/mol of hTK2 subunit, where dTTP > dCTP ≫ dATP) bound at the active site (*11*). In the present study, we have developed a purification protocol to successfully isolate an inhibitor-free enzyme, which retained the same pattern of oligomeric forms (i.e., mainly dimers and tetramers) as the previously characterized endogenously inhibited enzyme. The time course for the phosphorylation reaction catalyzed by the dNTP-inhibited hTK2 was characterized by a ∼5 min lag phase, which was completely removed by preincubation of the enzyme with substrates (*11*). The dNTP-free enzyme preparations revealed a linear time course, even in the absence of preincubation with the substrate or cosubstrate, which further confirms the complete absence of inhibitors bound to the enzyme. Moreover, the biphasic concentration dependences previously observed for the substrates dThd and dCyd, with two Hill coefficients calculated at different concentration ranges, become monophasic in the dNTP-free enzyme, demonstrating that the endogenous dNTP inhibitors accounted for the complex kinetic behavior. The dNTP-free oligomers revealed distinct kinetic properties, and the tetramer gave a ∼1.4-fold higher specific activity than the dimer, a slightly lower negative cooperativity toward dThd, and slightly higher $[S]_{0.5}$ values for the two substrates and cosubstrate (Figure 1 and Table 1). Moreover,

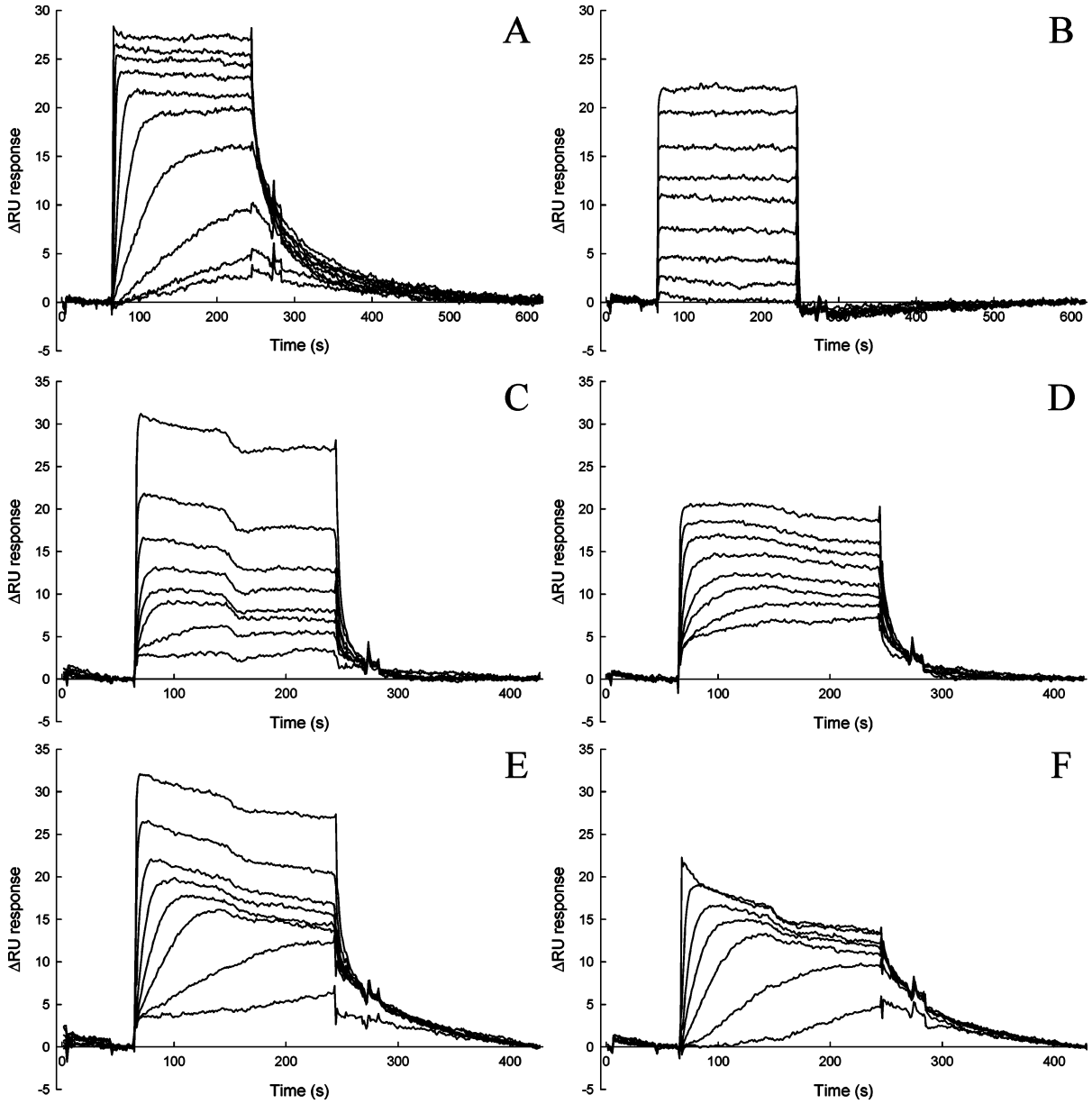

FIGURE 4: Sensorgrams of the interaction between dNTP-free immobilized dimeric hTK2 and increasing concentrations of dThd (A), dCyd (B), MgdTTP (C), dTTP (D), MgdCTP (E), and dCTP (F). The Mg^{2+}/dNTP ratio was 2:1 for the titrations where the divalent cation was present. Similar immobilization levels of the enzyme were obtained for all titrations, i.e., 16885 RU (A), 16562 RU (B), 18738 RU (C), 18019 RU (D), 17929 RU (E), and 18359 RU (F), consistent with 16.9, 16.6, 18.7, 18.0, 17.9, and 18.4 ng of enzyme/mm^2, respectively. The concentrations of dThd (A) are, from bottom to top, 2.5 nM, 5 nM, 10 nM, 25 nM, 50 nM, 0.1 μM, 0.25 μM, 0.5 μM, 2 μM, and 10 μM. The concentrations of dCyd (B) are, from bottom to top, 0.1 μM, 0.25 μM, 0.5 μM, 1 μM, 2 μM, 3 μM, 5 μM, 10 μM, and 15 μM. The concentrations of MgdTTP (C) and dTTP (D) are, from bottom to top, 10 nM, 25 nM, 50 nM, 0.1 μM, 0.25 μM, 0.5 μM, 2 μM, and 10 μM. The concentrations of MgdCTP (E) are, from bottom to top, 25 nM, 50 nM, 0.1 μM, 0.15 μM, 0.25 μM, 0.5 μM, 2 μM, and 10 μM. The concentrations of dCTP (F) are, from bottom to top, 25 nM, 50 nM, 0.1 μM, 0.15 μM, 0.25 μM, 0.5 μM, and 10 μM.

when compared to the dNTP-inhibited enzyme, the dNTP-free enzyme revealed a marked increase in the catalytic efficiency; i.e., it increased 16−18-fold with dThd and 10−11-fold with dCyd as the variable substrate.

Structural Stability of the dNTP-free hTK2 as Studied by Thermal Denaturation and Limited Proteolysis by Trypsin. Although ligand binding did not seem to induce significant alterations in the secondary structure of hTK2, we used CD-monitored thermal denaturation to probe for different conformational states assumed by the enzyme on binding different substrate and inhibitor compounds. Some proteins are capable of self-refolding *in vitro* upon thermal denaturation, but the occurrence of side reactions such as aggregation makes the denaturation of many proteins irreversible. As such, the thermal denaturation is often discussed in terms of the Lumry−Eyring model (*28*), in which a reversible unfolding step is followed by an irreversible denaturation step, $N \leftrightarrows U \rightarrow D$, where N, U, and D are the native, unfolded or partially unfolded, and denatured states of the protein, respectively (*29*, *30*). However, in many cases, an irreversible thermal denaturation can be successfully analyzed using simple irreversible models that are approximations to the Lumry−Eyring model (*22*, *29*, *31*−*33*). The CD-monitored thermal unfolding of hTK2 was found to be irreversible and was thus analyzed by the simple two-state irreversible model

$$N \xrightarrow{k} D$$

where k is a first-order rate constant that changes with temperature, as given by the Arrhenius equation. All denaturation curves measured with hTK2 could be perfectly fitted to eqs 2 and 3 describing this model (Figures 2 and 3), and because the enzyme shows both dimeric and tetrameric quaternary structures, the curves probably describe a process where dissociation and unfolding of the protein are occurring simultaneously. On the basis of the two-state irreversible model, the parameters of the Arrhenius equation were calculated, providing evidence for a significant structural stabilization of the enzyme (in terms of T_m) upon ligand binding, i.e., dCyd < MgdCTP < dThd < dCTP < dTTP < MgdTTP, whereas MgATP seemed to further destabilize hTK2. Despite the limited sequence homology, the similar structural fold and related catalytic properties of TK2 with other members of the nucleoside monophosphate kinase (NMPK) fold family, for which large ligand-induced conformational changes have been described, anticipate the occurrence of comparable motions also for this enzyme. Thus, on the basis of X-ray crystallographic studies, large conformational changes upon substrate binding have been described for adenylate kinase (ADK) (*34*, *35*) and uridine-cytidine kinase (UCK) (*36*) and are also known to occur for other members of the NMPK fold family, e.g. TK_{HSV1} (*37*), for which a thermal stabilization upon ligand binding was correlated with a large-scale conformational adaptation (*25*). Similarly, we show a remarkable ability of hTK2 to adopt different conformations, with defined thermal stabilities, on binding each specific ligand (Figure 3). In the ligand-free form, hTK2 dimer is ~11 °C more stable (in terms of T_m) than TK_{HSV1} (*25*). Moreover, while dThd induces a similar stabilization of the two enzymes (by ~12 and ~9 °C, respectively), the simultaneous addition of substrate and ATP had almost no further stabilizing effect on hTK2 ($\Delta T_m \approx +1$ °C), whereas an additional ~9 °C stabilization was reported for the virus enzyme (*25*). The most stable conformation was observed for the binary hTK2·MgdTTP complex, with a T_m value (79.9 °C) that was ~31 °C higher than the most unstable conformation assumed by the enzyme, i.e., in complex with the cosubstrate MgATP ($T_m = 49.0$ °C).

The fact that substrate/inhibitor binding to hTK2 results in major conformational changes is also supported by changes both in the susceptibility to limited tryptic proteolysis and in the ITF analyses (Table 3) of substrate/inhibitor-bound versus unliganded enzyme. The LID region in hTK2 contains a cluster of six positively charged residues (three arginines and three lysines) (*11*, *19*) and is intrinsically a key target for proteolysis by trypsin. Upon inhibitor binding, a closure of the LID region over the phosphate moiety will stabilize this structure in a more closed conformation (*20*) and partially protect it from proteolytic degradation by trypsin, explaining the higher resistance of the dNTP-inhibited enzyme to limited proteolysis. Moreover, the hydrogen bonding between the 3′ OH of the substrate dThd and Glu170 in the LID (*11*) is also expected to protect, to some extent, this structure from proteolytic degradation. Thus, incubation of the unliganded enzyme with this substrate increased its resistance to limited proteolysis.

Real-Time Binding Studies. The kinetics of the interactions between dNTP-free hTK2 dimer and its low-molecular-mass (227−507 Da) substrate and inhibitor compounds were also determined using the SPR biosensor technology. In general, their reversible binding resulted in an increase in the SPR signal, related to an increase in mass at the sensor surface, and a unique interaction kinetic profile was observed for each analyte (parts A−F of Figure 4 and Table 4). First, the apparent affinities confirmed that dThd is the preferred substrate and that dNTP-inhibitors bind with the highest affinities in the absence of Mg^{2+}. Second, the strong negative kinetic cooperativity of dThd binding ($h = 0.37$) was confirmed by the SPR analyses ($h = 0.31$). Finally, the slowest dissociation rate for the substrates was observed for the binding of dThd. Although, the mechanism of the negative cooperativity of dThd binding, in contrast to dCyd, has yet to be explained, it may be related to the difference in the association and dissociation rates observed for the two nucleosides by SPR (parts A and B of Figure 4 and Table 4). Unfortunately, the SPR analyses do not allow a determination of the number of binding sites for the nucleosides in the hTK2 dimer, because their specific refractive index increment (cm^3/g) versus the immobilized protein is not known. Similarly, dCTP takes a longer time to dissociate from hTK2 than dTTP (Table 4), and while dTTP is a regular noncooperative inhibitor of hTK2, dCTP inhibits the enzyme with complex negative cooperative kinetics (*38*, *39*).

Some of the sensorgrams were rather complex (parts C, E, and F of Figure 4) by demonstrating a reproducible instability of the association equilibrium signal at the higher concentrations of the analytes. The molecular basis for this instability has yet to be explained, but it may be related to the conformational flexibility of hTK2. Moreover, the ~4-fold increase in the measured association equilibrium signal [$\Delta RU_{max}/(ng/mm^2)$] observed for MgdTTP and MgdCTP as compared to dTTP and dCTP cannot be attributed solely to an increase in mass at the sensor surface caused by the additional binding of Mg^{2+} (24 Da). The observed differences in the SPR response may be explained alternatively by (i) a difference in the number of binding sites; i.e., dTTP and dCTP may bind with high affinity (Table 4) to only one of the two active sites in the dimer (half-of-the-site reactivity), whereas MgdTTP and MgdCTP bind with low affinity (Table 4) to both sites; (ii) the ~4-fold higher ΔRU response of the Mg complexes may be related to a conformational change of dimeric hTK2 because of a change in the dielectric properties of the enzyme−water matrix, as previously proposed for the SPR responses of rhodopsin (*40*), dihydrofolate reductase (*41*), phenylalanine hydroxylase (*42*), and maltose-binding protein and tissue transglutaminase (*43*); or (iii) other mechanisms, including a combination of the previous two alternatives. We cannot exclude the possibility that the inhibitors complexed with magnesium are also able to bind as a phosphate donor, with much lower affinity, in addition to the high-affinity binding as a "bisubstrate analogue" already observed by crystallization (*19*, *20*) and molecular docking (*11*). This alternative binding could explain both the decrease in affinity and in half-time of dissociation observed in the SPR experiments. It is interesting to note that the conformational change resulting from binding of the inhibitors to hTK2, as followed by ITF, showed the same apparent affinity and maximum response regardless of the presence of the counterion. It is possible, however, that the presence of magnesium does not bring any additional disturbance of specific (not identified) tryptophan residues

within the enzyme. Thus, whereas the ITF primarily reflects changes in the microenvironment of specific tryptophan residues in each subunit, the SPR response is intrinsically more complex and can reflect not only an increase in mass at the sensor chip surface upon analyte binding but also a global conformational change of the enzyme (*40*−*43*). This difference between the two probes may also explain the finding that hTK2 binds the natural substrates dThd and dCyd with negative cooperativity and a hyperbolic concentration dependence, respectively, as determined by steady-state kinetics and SPR spectroscopy, whereas the equilibrium binding isotherm obtained by ITF revealed a hyperbolic dependence for both substrates. Finally, it should be noted that the crystal structure of the related enzyme *Dm*-dNK, in complex with the inhibitor dTTP, contained a magnesium ion coordinating the β and γ phosphates of the nucleotide as well as some important amino acids (*20*). However, from our present data, it can be concluded that Mg^{2+} is not required for inhibitor (dTTP and dCTP) binding to hTK2.

CONCLUDING REMARKS

A detailed understanding of the catalytic and regulatory properties of the mitochondrial thymidine kinase (TK2) has so far been hampered by the complex enzyme kinetics displayed with its two main substrates, dThd and dCyd, when isolated from mammalian tissues (*39*, *44*, *45*) and as a recombinant protein from *E. coli* (*4*−*6*, *11*, *46*). Our recent discovery of tightly bound endogenous inhibitors (dNTPs) as the main source of the complex kinetics (*11*) is confirmed in the present study. Moreover, our procedure for the quantitative removal of the bound dNTPs, by displacement with high concentrations of dThd, has dramatically increased the catalytic efficiency of the enzyme and redefined some of its key kinetic and regulatory properties. The distinct kinetic properties of the two main substrates, dThd and dCyd, are confirmed by direct ligand-binding studies using ITF and SPR spectroscopy, all indicating that dThd is the preferred substrate. Moreover, dThd binds with a pronounced negative cooperativity, in contrast to dCyd, but further studies are required to explain the mechanism of this regulatory property. The dNTP-free recombinant hTK2 thus represents a key enzyme source for screening studies of nucleoside analogues, which have a broad pharmacological application as antiviral and anticancer agents.

Internal protein dynamics are intimately connected to enzyme catalysis. In the present study, experimental evidence is presented in support of different conformational states assumed by hTK2 in its ligand-free, substrate-bound, and dNTP-bound forms based on a number of independent spectroscopic techniques, i.e., ITF, far-UV CD, real-time SPR, and limited proteolysis by trypsin. No crystal structure of hTK2 is yet available, but from the high degree of sequence identity to the multisubstrate deoxynucleoside kinase *Dm*-dNK and the similarity in biochemical and biophysical characteristics between the two enzymes (*47*−*49*), comparable catalytic and regulatory properties, including feedback inhibition, are expected. Thus, the construction of a modeled dimeric hTK2 based on the known structure of *Dm*-dNK (*11*) and molecular dynamics simulations in the ligand-free form and in complex with dThd and MgdTTP have allowed the unveiling of the preliminary structural basis for the conformational changes observed experimentally. In the modeled ligand-free hTK2 and hTK2·dThd complex, large structural changes were observed at the active site and, in particular, large movements at the LID region and the P loop, initiating an opening of the active-site crevice, which is compatible with an induced fit mechanism of substrate binding (Barroso et al., unpublished data). Thus, future structural studies of hTK2 are expected to confirm the different conformations adopted by the enzyme on binding different physiological ligands as observed by the complementary biophysical methods in the present study.

REFERENCES

1. Arnér, E. S., and Eriksson, S. (1995) Mammalian deoxyribonucleoside kinases, *Pharmacol. Ther. 67*, 155−186.
2. Kit, S., and Leung, W. C. (1974) Submitochondrial localization and characteristics of thymidine kinase molecular forms in parental and kinase-deficient HeLa cells, *Biochem. Genet. 11*, 231−247.
3. Jansson, O., Bohman, C., Munch-Petersen, B., and Eriksson, S. (1992) Mammalian thymidine kinase 2. Direct photoaffinity labeling with [^{32}P]dTTP of the enzyme from spleen, liver, heart and brain, *Eur. J. Biochem. 206*, 485−490.
4. Wettin, K., Johansson, M., Zheng, X., Zhu, C., and Karlsson, A. (1999) Cloning of mouse mitochondrial thymidine kinase 2 cDNA, *FEBS Lett. 460*, 103−106.
5. Wang, L., and Eriksson, S. (2000) Cloning and characterization of full-length mouse thymidine kinase 2: The N-terminal sequence directs import of the precursor protein into mitochondria, *Biochem. J. 351*, 469−476.
6. Wang, L., Saada, A., and Eriksson, S. (2003) Kinetic properties of mutant human thymidine kinase 2 suggest a mechanism for mitochondrial DNA depletion myopathy, *J. Biol. Chem. 278*, 6963−6968.
7. Söderlund, J. C., and Arnér, E. S. (1994) Mitochondrial versus cytosolic activities of deoxyribonucleoside salvage enzymes, *Adv. Exp. Med. Biol. 370*, 201−204.
8. Johansson, M., and Karlsson, A. (1997) Cloning of the cDNA and chromosome localization of the gene for human thymidine kinase 2, *J. Biol. Chem. 272*, 8454−8458.
9. Johansson, M., Brismar, S., and Karlsson, A. (1997) Human deoxycytidine kinase is located in the cell nucleus, *Proc. Natl. Acad. Sci. U.S.A. 94*, 11941−11945.
10. Elholm, M., Hollås, H., Issalene, C., Barroso, J. F., Berge, R. K., and Flatmark, T. (2001) Transient up-regulation of liver mitochondrial thymidine kinase activity in proliferating mitochondria, *IUBMB Life 51*, 99−104.
11. Barroso, J. F., Elholm, M., and Flatmark, T. (2003) Tight binding of deoxyribonucleotide triphosphates to human thymidine kinase 2 expressed in *Escherichia coli*. Purification and partial characterization of its dimeric and tetrameric forms, *Biochemistry 42*, 15158−15169.
12. Saada, A., Shaag, A., Mandel, H., Nevo, Y., Eriksson, S., and Elpeleg, O. (2001) Mutant mitochondrial thymidine kinase in mitochondrial DNA depletion myopathy, *Nat. Genet. 29*, 342−344.
13. Carrozzo, R., Bornstein, B., Lucioli, S., Campos, Y., de la Pena, P., Petit, N., Dionisi-Vici, C., Vilarinho, L., Rizza, T., Bertini, E., Garesse, R., Santorelli, F. M., and Arenas, J. (2003) Mutation analysis in 16 patients with mtDNA depletion, *Hum. Mutat. 21*, 453−454.
14. Mancuso, M., Salviati, L., Sacconi, S., Otaegui, D., Camano, P., Marina, A., Bacman, S., Moraes, C. T., Carlo, J. R., Garcia, M., Garcia-Alvarez, M., Monzon, L., Naini, A. B., Hirano, M., Bonilla, E., Taratuto, A. L., DiMauro, S., and Vu, T. H. (2002) Mitochondrial DNA depletion: Mutations in thymidine kinase gene with myopathy and SMA, *Neurology 59*, 1197−1202.
15. Vila, M. R., Segovia-Silvestre, T., Gamez, J., Marina, A., Naini, A. B., Meseguer, A., Lombes, A., Bonilla, E., DiMauro, S., Hirano, M., and Andreu, A. L. (2003) Reversion of mtDNA depletion in a patient with TK2 deficiency, *Neurology 60*, 1203−1205.
16. Saada, A., Ben-Shalom, E., Zyslin, R., Miller, C., Mandel, H., and Elpeleg, O. (2003) Mitochondrial deoxyribonucleoside triphosphate pools in thymidine kinase 2 deficiency, *Biochem. Biophys. Res. Commun. 310*, 963−966.

17. Ikeda, S., Chakravarty, R., and Ives, D. H. (1986) Multisubstrate analogs for deoxynucleoside kinases. Triphosphate end products and synthetic bisubstrate analogs exhibit identical modes of binding and are useful probes for distinguishing kinetic mechanisms, *J. Biol. Chem. 261*, 15836−15843.
18. Kim, M. Y., and Ives, D. H. (1989) Human deoxycytidine kinase: Kinetic mechanism and end product regulation, *Biochemistry 28*, 9043−9047.
19. Johansson, K., Ramaswamy, S., Ljungcrantz, C., Knecht, W., Piškur, J., Munch-Petersen, B., Eriksson, S., and Eklund, H. (2001) Structural basis for substrate specificities of cellular deoxyribonucleoside kinases, *Nat. Struct. Biol. 8*, 616−620.
20. Mikkelsen, N. E., Johansson, K., Karlsson, A., Knecht, W., Andersen, G., Piškur, J., Munch-Petersen, B., and Eklund, H. (2003) Structural basis for feedback inhibition of the deoxyribonucleoside salvage pathway: Studies of the *Drosophila* deoxyribonucleoside kinase, *Biochemistry 42*, 5706−5712.
21. Andrade, M. A., Chacon, P., Merelo, J. J., and Moran, F. (1993) Evaluation of secondary structure of proteins from UV circular dichroism spectra using an unsupervised learning neural network, *Protein Eng. 6*, 383−390.
22. Kurganov, B. I., Lyubarev, A. E., Sanchez-Ruiz, J. M., and Shnyrov, V. L. (1997) Analysis of differential scanning calorimetry data for proteins. Criteria of validity of one-step mechanism of irreversible protein denaturation, *Biophys. Chem. 69*, 125−135.
23. Jönsson, U., Fägerstam, L., Ivarsson, B., Johnsson, B., Karlsson, R., Lundh, K., Löfås, S., Persson, B., Roos, H., Rönnberg, I., Sjölander, S., Stenberg, E., Ståhlberg, R., Urbaniczky, C., Östlin, H., and Malmqvist, M. (1991) Real-time biospecific interaction analysis using surface plasmon resonance and a sensor chip technology, *BioTechniques 11*, 620−627.
24. Hubbard, S. J. (1998) The structural aspects of limited proteolysis of native proteins, *Biochim. Biophys. Acta 1382*, 191−206.
25. Wurth, C., Kessler, U., Vogt, J., Schulz, G. E., Folkers, G., and Scapozza, L. (2001) The effect of substrate binding on the conformation and structural stability of Herpes simplex virus type 1 thymidine kinase, *Protein Sci. 10*, 63−73.
26. Sabini, E., Ort, S., Monnerjahn, C., Konrad, M., and Lavie, A. (2003) Structure of human dCK suggests strategies to improve anticancer and antiviral therapy, *Nat. Struct. Biol. 10*, 513−519.
27. Myszka, D. G. (2004) Analysis of small-molecule interactions using Biacore S51 technology, *Anal. Biochem. 329*, 316−323.
28. Lumry, R., and Eyring, E. (1954) Conformation changes of proteins, *J. Phys. Chem. 58*, 110−120.
29. Sanchez-Ruiz, J. M. (1992) Theoretical analysis of Lumry−Eyring models in differential scanning calorimetry, *Biophys. J. 61*, 921−935.
30. Plaza del Pino, I. M., Ibarra-Molero, B., and Sanchez-Ruiz, J. M. (2000) Lower kinetic limit to protein thermal stability: A proposal regarding protein stability *in vivo* and its relation with misfolding diseases, *Proteins 40*, 58−70.
31. Milardi, D., La Rosa, C., and Grasso, D. (1994) Extended theoretical analysis of irreversible protein thermal unfolding, *Biophys. Chem. 52*, 183−189.
32. Lyubarev, A. E., and Kurganov, B. I. (1998) Modeling of irreversible thermal protein denaturation at varying temperature. I. The model involving two consecutive irreversible steps, *Biochemistry (Moscow) 63*, 434−440.
33. Lyubarev, A. E., and Kurganov, B. I. (1999) Modeling of irreversible thermal protein denaturation at varying temperature. II. The complete kinetic model of Lumry and Eyring, *Biochemistry (Moscow) 64*, 832−838.
34. Schulz, G. E., Müller, C. W., and Diederichs, K. (1990) Induced-fit movements in adenylate kinases, *J. Mol. Biol. 213*, 627−630.
35. Vonrhein, C., Schlauderer, G. J., and Schulz, G. E. (1995) Movie of the structural changes during a catalytic cycle of nucleoside monophosphate kinases, *Structure 3*, 483−490.
36. Suzuki, N. N., Koizumi, K., Fukushima, M., Matsuda, A., and Inagaki, F. (2004) Structural basis for the specificity, catalysis, and regulation of human uridine-cytidine kinase, *Structure 12*, 751−764.
37. Perozzo, R., Jelesarov, I., Bosshard, H. R., Folkers, G., and Scapozza, L. (2000) Compulsory order of substrate binding to herpes simplex virus type 1 thymidine kinase. A calorimetric study, *J. Biol. Chem. 275*, 16139−16145.
38. Lee, L. S., and Cheng, Y. (1976) Human deoxythymidine kinase II: Substrate specificity and kinetic behavior of the cytoplasmic and mitochondrial isozymes derived from blast cells of acute myelocytic leukemia, *Biochemistry 15*, 3686−3690.
39. Munch-Petersen, B., Cloos, L., Tyrsted, G., and Eriksson, S. (1991) Diverging substrate specificity of pure human thymidine kinases 1 and 2 against antiviral dideoxynucleosides, *J. Biol. Chem. 266*, 9032−9038.
40. Salamon, Z., Wang, Y., Brown, M. F., Macleod, H. A., and Tollin, G. (1994) Conformational changes in rhodopsin probed by surface plasmon resonance spectroscopy, *Biochemistry 33*, 13706−13711.
41. Sota, H., Hasegawa, Y., and Iwakura, M. (1998) Detection of conformational changes in an immobilized protein using surface plasmon resonance, *Anal. Chem. 70*, 2019−2024.
42. Flatmark, T., Stokka, A. J., and Berge, S. V. (2001) Use of surface plasmon resonance for real-time measurements of the global conformational transition in human phenylalanine hydroxylase in response to substrate binding and catalytic activation, *Anal. Biochem. 294*, 95−101.
43. Gestwicki, J. E., Hsieh, H. V., and Pitner, J. B. (2001) Using receptor conformational change to detect low molecular weight analytes by surface plasmon resonance, *Anal. Chem. 73*, 5732−5737.
44. Munch-Petersen, B. (1984) Differences in the kinetic properties of thymidine kinase isoenzymes in unstimulated and phytohemagglutinin-stimulated human lymphocytes, *Mol. Cell. Biochem. 64*, 173−185.
45. Munch-Petersen, B., Völker, C., Cloos, L., Hofbauer, R., Mortensen, B. T., and Tyrsted, G. (1994) Altered substrate and inhibitor specificity of purified human adult thymidine kinases (TK2) from leukemic cells, *Adv. Exp. Med. Biol. 370*, 253−256.
46. Wang, L., Munch-Petersen, B., Herrström Sjöberg, A., Hellman, U., Bergman, T., Jörnvall, H., and Eriksson, S. (1999) Human thymidine kinase 2: Molecular cloning and characterisation of the enzyme activity with antiviral and cytostatic nucleoside substrates, *FEBS Lett. 443*, 170−174.
47. Munch-Petersen, B., Piškur, J., and Søndergaard, L. (1998) The single deoxynucleoside kinase in *Drosophila melanogaster*, *Dm*dNK, is multifunctional and differs from the mammalian deoxynucleoside kinases, *Adv. Exp. Med. Biol. 431*, 465−469.
48. Munch-Petersen, B., Piškur, J., and Søndergaard, L. (1998) Four deoxynucleoside kinase activities from *Drosophila melanogaster* are contained within a single monomeric enzyme, a new multifunctional deoxynucleoside kinase, *J. Biol. Chem. 273*, 3926−3931.
49. Johansson, M., van Rompay, A. R., Degrève, B., Balzarini, J., and Karlsson, A. (1999) Cloning and characterization of the multisubstrate deoxyribonucleoside kinase of *Drosophila melanogaster*, *J. Biol. Chem. 274*, 23814−23819.

BI047766M